

## **VIII- II -1. Project Research**

### **Project 12**

## PR12 Irradiation Effects on Microstructural Evolution in Materials Irradiated by Particles with High Energy

Q. Xu

*Research Reactor Institute, Kyoto University*

**OBJECTIVES:** Neutron irradiation is important to develop nuclear materials and to understand the mechanism of microstructural evolution in solid materials under irradiation conditions. Kyoto University research reactor was available to be used after low-enriched uranium core change, which took almost four years. In addition, other irradiation fields in the Research Reactor Institute, such as ions, electrons and  $\gamma$  rays, have also been used in the present project research to clarify the damage structural development.

**RESULTS:** The allotted research subject (ARS) and the name of co-researches in each ARS are listed below. A number of important data were already obtained. Details are presented in this progress reports.

### ARS-1

Thermally stimulated current studies on electron-irradiated single crystal ZnO bulk: dual light illumination effect

(K. Kuriyama, Y. Izawa, T. Oga, K. Kushida, and Q. Xu)

### ARS-2

Surface structure change in heavy ion irradiated GaSb and InSb

(N. Nitta, T. Hasegawa, H. Yasuda, Y. Hayashi, T. Yoshiie, M. Taniwaki and H. Mori)

### ARS-3

Study on formation and recovery of damage in irradiated crystalline materials

(A. Kinomura, Y. Nakano, Q. Xu and T. Yoshiie)

### ARS-4

Thermoluminescence of calcites irradiated by gamma rays

(T. Awata and Q. Xu)

### ARS-5

Correlation between thermal diffusivity and positron an-

nihilation lifetime of ceramics irradiated by neutron and 30MeV electron

(M. Akiyoshi, I. Takagi, T. Yoshiie, Q. Xu, K. Sato)

### ARS-6

Electron-irradiation effects on Cr precipitates in a Cu-Cr-Zr alloy studied by three-dimensional atom probe (Y. Nagai, T. Toyama, M. Hatakeyama, Y. Matsukawa, Y. Shimizu, A. Kuramoto, H. Takamizawa, K. Saito, T. Yoshiie, Q. Xu)

### ARS-7

Defects study for bulk metallic glass alloys damaged by electron irradiation

(F.Hori, N.Onodera, M.Marubishi, A.Ishii, S.Mineno, A.Iwase, Q.Xu, K.Sato and T.Yoshiie)

### ARS-8

Microstructure of neutron irradiated vanadium alloys in a liquid sodium environment

(K. Fukumoto, M. Iwasaki and Q. Xu)

### ARS-9

Damage evolution in neutron-irradiated metals during neutron irradiation at elevated temperatures

(I. Mukouda, K. Yamakawa, T. Yoshiie, Q. Xu)

### ARS-10

Effects of thermal aging on mechanical properties of Fe-Cr ferritic alloys

(R. Kasada, Y. Sakamoto, K. Yabuuchi, A. Kimura, K. Sato, Q. Xu, T. Yoshiie<sup>3</sup>)

### ARS-11

Microstructure studies of hydrogen-loaded nanocrystalline Ni

(H. Tsuchida, A. Itoh, K. Sato, T. Yoshiie, Q. Xu)

### ARS-12

Eetection of deuterium trapped at vacancy-type defects by positron annihilation spectroscopy

(K. Sato, K. Takeyasu, Q. Xu, K. Mori and T. Yoshiie)

### ARS-13

Hydrogen retention in tungsten materials

(K. Tokunaga, K. Araki, T. Fujiwara, Y. Miyamoto, Q. Xu, T. Yoshiie)

K. Kuriyama, Y. Izawa, T. Oga, K. Kushida<sup>1</sup> and Q. Xu<sup>2</sup>

*College of Engineering and Research Center of Ion Beam Technology, Hosei University*

<sup>2</sup>*Osaka Kyoiku University*

<sup>3</sup>*Research Reactor Institute, Kyoto University*

**INTRODUCTION:** Thermally stimulated current (TSC) method is used for investigating the energy levels of defects and/or impurities in high resistive bulk ZnO single crystals. However, conventional TSC studies using white light [1] or monochromatic light LEDs [2, 3] cannot discriminate the electron trap from the hole trap. In order to determine the donor like or acceptor like defects, we carried out the dual light illumination, namely the illumination with wavelength near the band gap and subsequent illumination with wavelength below the band gap. The measurements using blue ( $\lambda=465\text{nm}$ ) or red LED ( $\lambda=644\text{ nm}$ ) for excitation near or below the band gap were also performed.

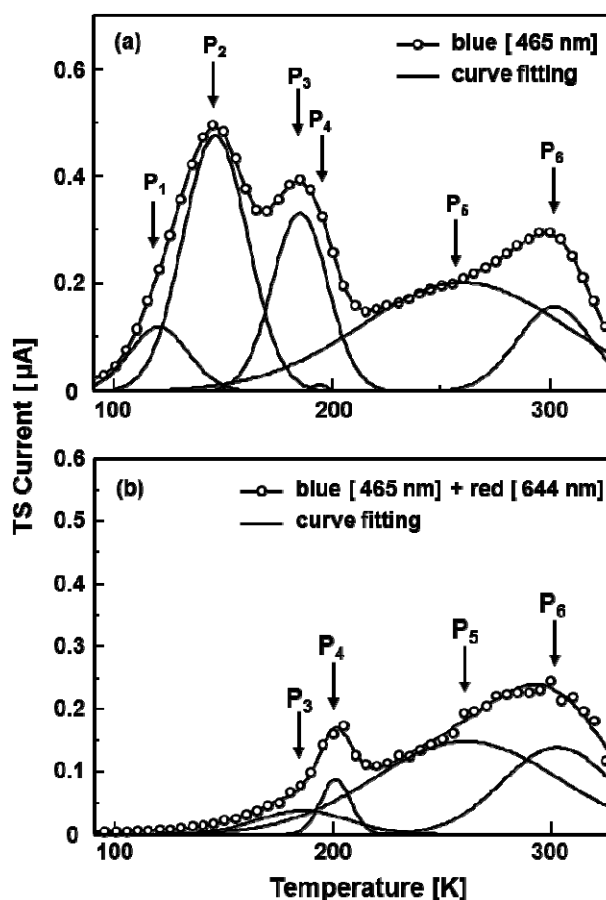
**EXPERIMENT:** ZnO single crystal used in this study were grown by the hydrothermal method. c-face cut ZnO samples showed high resistivities of  $10^3\text{-}10^5\ \Omega\text{cm}$ . Electron irradiation was carried out at room temperature with 30-MeV electrons using an electron linear accelerator facility at Kyoto University Research Institute. The irradiation dose was  $1 \times 10^{17}\ \text{cm}^{-2}$ . The bias voltage of 20 V was applied to the Al and Au alloy electrodes for the TSC measurements using Van der Pauw technique. TSC measurements performed at 90K using LEDs with various wavelengths.

**RESULTS:** As shown in Fig.1 (a), these broad peaks taken for excitation using a blue LED were resolved to optimum Gaussian curves, leading to six traps, P<sub>1</sub> ( $T_m=120\text{ K}$ ), P<sub>2</sub> (146 K), P<sub>3</sub> (185 K), P<sub>4</sub> (194 K), P<sub>5</sub> (260 K), and P<sub>6</sub> (302 K). According to the approximate relationship [4]  $E_i \approx kT_m \ln(T_m^4/\beta)$ , where  $E_i$  is the ionization energy,  $k$  Boltzmann's constant,  $T_m$  the TSC peak temperature,  $\beta$  the heating rate for the thermal scan. The ionization energies for these traps were calculated to be  $E_i(P_1) = 149$ ,  $E_i(P_2) = 256$ ,  $E_i(P_3) = 317$ ,  $E_i(P_4) = 381$ ,  $E_i(P_5) = 525$ , and  $E_i(P_6) = 650\ \text{meV}$ .  $E_i$  values estimated by the present TSC study contain an uncertainty of  $\pm 20\ \text{meV}$ . The origin of the P<sub>2</sub> and P<sub>3</sub> traps has been attributed to the Li acceptor [2] and oxygen vacancy [1, 2], respectively. The TS current for P<sub>5</sub> and P<sub>6</sub> traps was also assigned to the zinc vacancy and interstitial oxygen, respectively [3]. Fig.1 (b) shows that P<sub>1</sub>, P<sub>2</sub>, and P<sub>3</sub> traps disappeared by the dual light illumination (blue LED illumination and subsequent red LED illumination), while P<sub>4</sub>, P<sub>5</sub>, and P<sub>6</sub> traps remained.

The electrons in defects captured by the blue LED illumination would be swept out to the conduction band

by the subsequent illumination using a red LED. It is suggested that P<sub>1</sub>, P<sub>2</sub> and P<sub>3</sub> traps are the donor like defects located near the conduction band, while P<sub>4</sub>, P<sub>5</sub>, and P<sub>6</sub> traps are the acceptor like defect located near the valence band. Therefore, the Li acceptor introduced during the crystal growth might be related to P<sub>4</sub> rather than P<sub>2</sub> traps.

Fig. 1. (a) TSC spectra resolved to six traps for the excitation using a blue LED and (b) four traps for the excitation using the dual light illumination (blue LED and subsequent red LED illumination).



### REFERENCES:

- [1] Z.-Q. Fang, B. Clafin, D.C. Look, G.C. Farlow, J. Appl. Phys. 101 (2007) 086106.
- [2] K. Kuriyama, M. Ooi, K. Matsumoto, K. Kushida, Appl. Phys. Lett. 89 (2006) 242113.
- [3] K. Kuriyama, K. Matsumoto, Y. Suzuki, K. Kushida, and Q. Xu, Solid State Commun. 149, 1347 (2007).
- [4] D.C. Look, Semicond. Semimet. 19 (1983) 75.

## PR12-2 Surface Structure Change in Heavy Ion Irradiated GaSb and InSb

N. Nitta, T. Hasegawa, H. Yasuda, Y. Hayashi, T. Yoshiie<sup>1</sup>,  
M. Taniwaki<sup>2</sup> and H. Mori<sup>3</sup>

*Department of Mechanical Engineering, Kobe University,  
Japan*

<sup>1</sup>*Research Reactor Institute, Kyoto University,, Japan*

<sup>2</sup>*School of Environmental Science and Technology, Kochi  
University of Technology, Japan*

<sup>3</sup>*Research Center for Ultra-High Voltage Electron Mi-  
croscopy, Osaka University, Japan*

### 1. Introduction

Three types of defect structure formation have been observed in ion irradiated III-V compound semiconductors. Typical defect structure formation occurs in many semiconductors (Si, GaAs, InP etc.), in which a damaged layer corresponding to the projected ion range is formed on the surface; further irradiation transforms the damaged layer into an amorphous structure. In the case of GaN, nitrogen bubbles and gallium nanocrystals are formed in the amorphized layer by ion irradiation. In GaSb and InSb, anomalous behaviors, such as elevation, swelling, and the formation of holes, voids, nanofibers, and cellular structures with nanometer to submicron dimensions, are observed on irradiated surfaces. Similar phenomena occur in irradiated Ge surfaces. It has been clarified that such anomalous phenomena occur as a result of the movement of point defects induced by ion irradiation, and that these structures are generated after void formation. These phenomena have been reported in relation to bulk irradiation. Thin film irradiation will yield some useful knowledge on the movement of point defects utilizing surface sinks; however there are few studies on GaSb and InSb. In this study, void formation in the early stage of such structures and structure change by ion irradiation were investigated in GaSb and InSb thin films using transmission electron microscopy (TEM). In addition, structures formed in GaSb were compared with those formed in InSb in order to investigate the effect of the constituent elements.

### 2. Experimental procedures

Single crystals of GaSb and InSb were supplied in the form of wafers 450 mm thick with the <001> normal. Then the disks with a 3 mm diameter cut from the single crystals were mechanically polished and thinned by ion milling with argon for TEM observation. Sn<sup>+</sup> ion irradiation of 60 keV was performed for thin film at room tem-

perature using a heavy ion accelerator in KUR. The projected ion range was 25 nm in GaSb and 27 nm in InSb, obtained by the stopping and range of ions in matter (SRIM) code simulation. The ion dose and flux were  $0.25 \times 10^{18}$  -  $2 \times 10^{18}$  ions/m<sup>2</sup> and  $3 \times 10^{11}$  ions/m<sup>2</sup>s, respectively. The observation was carried out with a transmission electron microscope (HITACHI H-7000 and HF-2000) operated at 125 kV and 200 kV.

### 3. Results

The voids were formed after irradiation in both GaSb and InSb. In the case of GaSb irradiated to a dose of  $0.25 \times 10^{18}$  ions/m<sup>2</sup>, the density of voids was  $3 \times 10^{15}$  voids/m<sup>2</sup> and their average diameter was about 14 nm. The swelling ratio of voids was 9 % (a damage level of approximately 0.75 dpa). The diameter of voids grew to 23 nm in the sample irradiated to a dose of  $0.5 \times 10^{18}$  ions/m<sup>2</sup>. The density of voids was  $2 \times 10^{15}$  voids/m<sup>2</sup>. Despite the increasing ion dose, the density decreased, which seems to be due to the coalescence of several voids. The swelling of voids increased up to 24 % (a damage level of approximately 1.5 dpa). The average diameter, density, and swelling ratio of the voids were about 22 nm,  $2 \times 10^{15}$  voids/m<sup>2</sup>, and 24 % (a damage level of approximately 3 dpa) in the  $1 \times 10^{18}$  ions/m<sup>2</sup> sample, and about 21 nm,  $2 \times 10^{15}$  voids/m<sup>2</sup>, and 17 % (a damage level of approximately 6 dpa) in the  $2 \times 10^{18}$  ions/m<sup>2</sup> sample, respectively. With increasing ion dose, the void diameter increased under low irradiation doses. However, the diameter did not change significantly under high irradiation. It is considered that newly formed voids play a role in the surface sink. The formed interstitials and vacancies escape to the void surface; therefore, voids do not grow under high irradiation. The average diameter of the voids in InSb irradiated with 60 keV Sn<sup>+</sup> ions to a dose of  $0.25 \times 10^{18}$  ions/m<sup>2</sup> was about 20 nm at room temperature. The void size in InSb is larger than that in GaSb. The large void size is quantitatively explained by the amount of induced vacancies obtained by the SRIM code simulation.

The Debye-Scherrer rings were observed in the SAED patterns on both materials. The structure changes into a polycrystal by ion irradiation. Additionally, the 200 superlattice reflections in the [001] net pattern of InSb were almost absent, and the streak pattern along the <110> direction was observed in InSb. It is considered that the anti phase domains of different lengths are formed by ion irradiation. Ion irradiation transforms the structure of InSb from chemical ordering to chemical disordering via the formation of anti phase boundaries.

---

採択課題番号 22P12-2 半導体イオン照射によって導入される点欠陥挙動の解明と プロジェクト  
ナノセル技術の開発

(高知工科大・環境) 谷脇雅文、(神戸大・工) 新田紀子、(京大・原子炉) 義家敏正、徐 虬

## PR12-3 Study on Formation and Recovery of Damage in Irradiated Crystalline Materials

A. Kinomura, Y. Nakano<sup>1</sup>, Q. Xu<sup>1</sup> and T. Yoshiie<sup>1</sup>

National Institute of Advanced Industrial Science and Technology (AIST)

<sup>1</sup>Research Reactor Institute, Kyoto University

**INTRODUCTION:** The effects of ion irradiation damage have been extensively studied for various materials. However, residual defects experimentally detected are often less than primary defects theoretically calculated. It implies that both damaging and recovery processes coexist during irradiation. A typical case of the recovery effect is the ion beam annealing in Si, where implantation-induced damage layers are recrystallized under other ion irradiation at elevated temperatures. It is important to investigate the competing processes for the application and fundamental studies on interactions of energetic particles (ions and neutrons) with materials. This study aims to investigate such radiation effects in ion-irradiated crystalline materials.

**EXPERIMENTS:** Two types of samples were studied in this year: (1) Hydrogen-implanted multicrystalline Si to observe the gettering of metal impurities to hydrogen-induced nanocavities; (2) neutron-irradiated single-crystalline Si to investigate the damage recovery of ion-implanted layers. Some of these irradiated samples were already characterized by neutron activation analysis and/or Rutherford backscattering/channeling (RBS/C). We performed cross-sectional transmission electron microscopy (TEM) to understand the nature of the radiation damage. It is difficult to make thinned samples for cross-sectional TEM observation, when the amount of samples are limited like this study. To obtain sufficient TEM samples from the limited amount of samples, we used an FIB (focused ion beam) milling system. The FIB milling method is also good for multicrystalline samples as sampling points can be easily chosen from inner-grain or grain-boundary regions. The TEM observation was performed with a 200 keV electron beam.

**RESULTS:** The multicrystalline Si observed was implanted with 50 keV H<sup>+</sup> to a dose of 3×10<sup>16</sup> H<sup>+</sup>/cm<sup>2</sup> followed by annealing at 850 °C for 1h [1]. A cross-sectional TEM sample was cut from the center of a grain and put on a Cu grid by using a precisely adjustable manipulator. A Pt protective layer was deposited on the sampling point prior to the cutting process to protect the surface side of the cross-sectional sample during the FIB

milling. The thickness of the sample was about 2 μm and thinned by FIB milling down to electronically transparent thickness. Fig. 1 shows the TEM sample after the FIB milling. The lower left-hand side corresponds to the surface side. The black part of the upper right-hand side is the edge of the Cu grid. Although the Pt protective layer was missing together with some of the sample near the surface, the thickness of the sample was sufficiently uniform. In the detailed observation with higher magnification, nanocavities were found in this sample. A preliminary RBS measurement of the hydrogen-implanted sample after Au gettering suggested that hydrogen-induced cavities are formed in multicrystalline samples as well as the single crystalline samples. The TEM result of this study confirmed the RBS result more directly.

TEM samples were prepared by the FIB milling in the same way as the multicrystalline Si sample. A damage layer was introduced by self-ion (Si<sup>+</sup>) implantation at 200 keV to a dose of 5×10<sup>14</sup> cm<sup>-2</sup> before the neutron irradiation in the case of this sample. The TEM images indicated the damage layer around the projected range of Si ions. Further investigation on the neutron-irradiated samples is in progress.

In summary, the TEM sample preparation by the FIB milling was performed for single- and multicrystalline-Si samples in this study. Without any additional sample treatments such as chemical etching, the ion implanted layers were successfully observed.

**ACKNOWLEDGMENT:** We would like to thank Dr. Sato (KURRI) and colleagues in AIST for their assistance on this study.

[1] A. Kinomura, Y. Horino, Y. Nakano and J. S. Williams, J. Appl. Phys. 98 (2005) 066102.

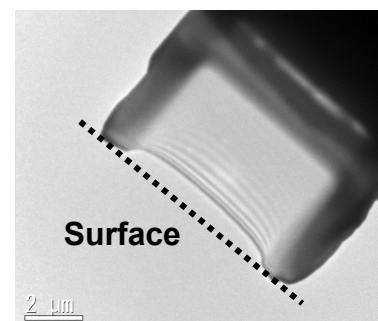


**Fig. 1.** Cross-sectional TEM image of the H-implanted Si sample prepared by FIB milling.

T. Awata and Q. Xu<sup>1</sup>

Department of Physics, Naruto University of Education  
<sup>1</sup>Research Reactor Institute, Kyoto University

**INTRODUCTION:** In order to clear the history and/or dating of the rocks, minerals and soils, the thermoluminescence measurement is one of the most important method in the field of the geology. Especially, the calcite ( $\text{CaCO}_3$ ) that is a core mineral of marble and limestone has been studied by many scientists from the latter half of 1940's[1-3], because the intensity of thermoluminescence of its is higher than other famous minerals and it has the possibility to apply the radiation dosimeter. V. Ponnusamy et al. [4] reported that the intensity of luminescence of blue- calcite which was irradiated by  $\gamma$  rays was depend on the annealing treatments and the emission spectra of all samples have an emission band at 610nm, and might be assumed that the recombination are always in involves  $\text{Mn}^{2+}$  ions. Macedo et al. [5] reported the  $\text{Mn}^{2+}$  ion was the mainly luminescence center in calcite even for any doped samples such as  $\text{CaCO}_3:\text{Sr}^{2+}$ , and  $\text{Mn}^{2+}$  was playing a important role of emission at around 610nm. In this study, we have performed experiments of thermoluminescence measurements for color calcites with different impurities irradiated  $\gamma$  rays to clear the relationship with emission bands and impurities of calcite.

**EXPERIMENTS:** The experiments were carried out using  $^{60}\text{Co}$   $\gamma$  rays irradiation facility at KUR. The samples were some natural calcites and those were irradiated by  $\gamma$  rays for 1h (20kGy) at 77K. The thermoluminescence spectra were measured by a photo-spectrometer (Princeton Instrument Spectra Pro 300i) with a temperature controlled system. Impurity elements were analyzed using an X-ray Fluorescence Spectroscopy (Rigaku RIX2000).

**RESULTS:** Figure 1 showed a 3D thermoluminescence spectra of pink calcite irradiated by  $\gamma$  rays at 77K from 93K to 413K with heating speed at 0.32K/sec. X-, Y-, and Z indicate emission wavelength (nm) of emission, temperature and intensity, respectively. There

is only one orange emission peak at 620nm with at 180K, 227K and above 349K. Results from XRF analysis of pink calcite, the mass concentrations of impurities were 90ppm for Sr, 70ppm for Cu, 130ppm for Mn, respectively. Orange the orange emission around 620nm is originated from the electron transition from  $^4G$  to  $^6S$  state of  $\text{Mn}^{2+}$ .

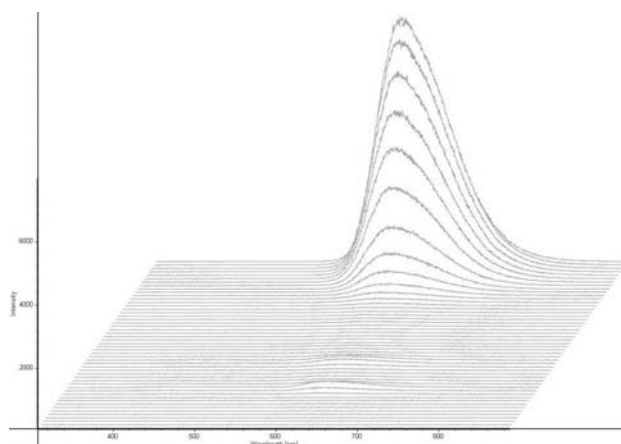


Fig.1. Thermoluminescence spectra of pink calcite irradiated by  $\gamma$  rays at 77K from 93K to 413K.

#### REFERENCES:

- [1] W. L. Medlin, *J. Opt. Soc. Am.* 53(1963) 1276-1285.
- [2] W. L. Medlin, *J. Chem. Phys.* **30**, pp451-458 (1959).
- [3] W. L. Medlin, *Phys. Rev.* **135**, pp.A1770 (1964).
- [4] V. Ponnusamy, V. Ramasamy, M. Dheenathayalu, et al., *Nucl. Instr. and Meth. B* **217** (2004)611-620.
- [5] Z. S. Macedo, M. E. G. Valerio and J. F. de Lima, *J. Phys. Chem. Solids* **60** (1999) 1973-1981.

M. Akiyoshi<sup>1</sup>, I. Takagi<sup>1</sup>, T. Yoshiie<sup>2</sup>, Q. Xu<sup>2</sup> and K. Sato<sup>2</sup>

<sup>1</sup>Faculty of Engineering, Kyoto University

<sup>2</sup>Research Reactor Institute, Kyoto University

## INTRODUCTION:

Measurement of thermal diffusivity and positron annihilation lifetime were performed on neutron and 30MeV electron irradiated ceramics. Thermal diffusivity of heavily neutron irradiated ceramics was decreased to very low level and the difference between specimens was small. Positron annihilation lifetime of these specimens showed also distinct change, but the difference between specimens were also small. So in this study, electron irradiation was performed to 0.01-0.02 dpa via 30MeV KURRI-Linac. The electron irradiated specimens also showed obvious degradation in thermal diffusivity and increment in positron annihilation lifetime, and it was clarified that positron annihilation lifetime showed some correlation with thermal diffusivity.

## EXPERIMENTS:

Typical structural ceramics ( $\alpha$ -Al<sub>2</sub>O<sub>3</sub>, AlN,  $\beta$ -Si<sub>3</sub>N<sub>4</sub> and  $\beta$ -SiC) were irradiated by 30MeV electron using the KURRI-LINAC up to  $1.5 \times 10^{24} \text{ e/m}^2$  (correspond to 0.01dpa) at 300K in the water-cooled specimen holder. This dose, 0.01dpa, was enough to induce significant degradation in thermal diffusivity. Thermal diffusivity was measured by laser flash method in the previous work, and that showed about 20%, 40%, 30%, 75% degradation for  $\alpha$ -Al<sub>2</sub>O<sub>3</sub>, AlN,  $\beta$ -Si<sub>3</sub>N<sub>4</sub> and  $\beta$ -SiC respectively.

Positron annihilation lifetime was also measured using conventional  $\gamma$ - $\gamma$  fast coincidence method in Radiation Laboratory, Uji. The irradiated specimen was  $\phi 10 \times 2 \text{ mm}$  or  $\phi 3 \times 0.5 \text{ disk}$ , and the number of the specimen was only one for each material. Usually,  $\gamma$ - $\gamma$  coincidence PAL method requires two peaces of specimens to put a positron source between specimens. In this work, we used one peace of non-irradiated specimen at the other side of the irradiated specimen. Positron source was specially ordered 1MBq <sup>22</sup>Na sealed by Ti foil, and the active diameter was 1mm.

The obtained PAL spectrum was analyzed with PALSfit program, with resolution FWHM about 300 ps at first and now achieved 230ps. In analyze of the spectrum, a source component that represents annihilation in the Ti foil was not resolved, and only two or three component was guessed in the analysis.

## RESULTS:

After the spectrum analysis, average positron lifetime  $\langle \tau \rangle$  was obtained as  $\langle \tau \rangle = \tau_1 I_1 + \tau_2 I_2$ , where  $\tau_i$  are the analyzed positron lifetimes and  $I_i$  are the intensities for the components. The average lifetime  $\langle \tau \rangle$  of electron irradiated  $\alpha$ -Al<sub>2</sub>O<sub>3</sub> and AlN indicated significant incre-

ment same as neutron irradiated specimens. On the other hand,  $\beta$ -Si<sub>3</sub>N<sub>4</sub> and  $\beta$ -SiC showed almost no change in lifetime same as neutron irradiated specimen.

At last, average positron lifetime was compared with thermal diffusivity. Fig.1 shows the result in  $\alpha$ -Al<sub>2</sub>O<sub>3</sub> and  $\beta$ -SiC irradiated by electron or neutron. It is noticed that the origin of specimen for electron irradiation and neutron irradiation was different and thermal diffusivity and  $\langle \tau \rangle$  was different even in the unirradiated specimen.

$\alpha$ -Al<sub>2</sub>O<sub>3</sub> showed most close correlation between thermal diffusivity and PAL. On the other hand, the thermal diffusivity of unirradiated specimen was no so high, while unirradiated AlN showed very high thermal diffusivity that make easy to evaluate the difference after an electron irradiation. And several commercial SiC specimens show high thermal diffusivity, so n-type SiC is also considered to be candidate to estimate the dynamic irradiation effect.

With these study, 30MeV electron Linac is confirmed to be very suitable device for irradiation.

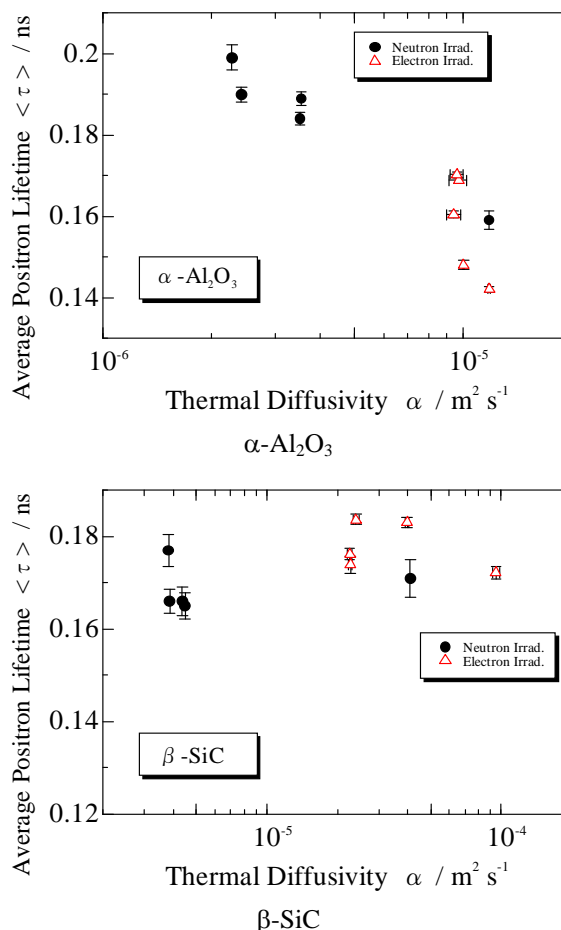


Fig.1. Change of average positron lifetime in electron and neutron irradiated ceramics compared with thermal diffusivity.

Y. Nagai<sup>1</sup>, T. Toyama<sup>1</sup>, M. Hatakeyama<sup>1</sup>, Y. Matsukawa<sup>1</sup>,  
Y. Shimizu<sup>1</sup>, A. Kuramoto<sup>1</sup>, H. Takamizawa<sup>1</sup>, K. Saito<sup>1</sup>, T.  
Yoshiie<sup>2</sup> and Q. Xu<sup>2</sup>

<sup>1</sup>Institute for Materials Research, Tohoku University

<sup>2</sup>Research Reactor Institute, Kyoto University

**INTRODUCTION:** Cu-Cr-Zr alloy is expected as a potential heat sink material of the International Thermonuclear Experimental Reactor (ITER) divertor because of its high electrical conductivity and simultaneously high strength. The high conductivity is due to the very low solubility of Cr and Zr in the Cu matrix, whereas, the high strength is due to particle-dispersion strengthening by Cr precipitation after thermal aging process. We have recently studied the Cu-Cr-Zr alloys irradiated in KUR-LINAC using positron annihilation spectroscopy and revealed that Cr-free defects are induced in the Cu matrix [1]. In this study, we investigate the irradiation effects on the Cr precipitates using three-dimensional atom probe (3D-AP) to reveal fundamental information on the evolution and the stability of the Cr precipitates.

**EXPERIMENTAL:** The chemical composition of the studied material is Cu-0.78Cr-0.13Zr-0.008Fe-0.003Si (wt.%). The samples were solution annealed at 960 °C for 3h followed by water-quenching, then aged at 460 °C for 3h and 600 °C for 1h. The details of the heat treatment are described in refs. [2, 3]. Cr precipitates of about 3 nm in diameter were formed and dispersed homogeneously before irradiation. The samples were irradiated at 77K by 28MeV electrons to a fluence of about  $1 \times 10^{19}$  e/cm<sup>2</sup> using the KUR-LINAC. 3D-AP samples were prepared by electro-polishing and focused ion beam milling. 3D-AP observations were carried out on a LEAP-3000XHR instrument, applying a laser power of 0.5 nJ, a laser pulse repetition rate of 200 kHz, a DC voltage in a range from 6 to 8 kV and a specimen temperature of 50 K.

**RESULTS & DISCUSSION:** Figure 1 shows the 3D atom map of Cr in the irradiated Cu-Cr-Zr alloy. Cr precipitates are clearly observed in high number density. The average diameter and the number density of the precipitates are 3.0 nm and  $2.1 \times 10^{18}$  /cm<sup>3</sup>, respectively. They are in good agreement with those obtained in unirradiated sample: 2.8 nm and  $2.0 \times 10^{17}$  /cm<sup>3</sup> [2, 3], suggesting that no marked irradiation-induced precipitation is formed. Fig.2 shows the one dimensional concentration profiles

of Cr, Zr, Fe and Si around a precipitate in the irradiated and unirradiated Cu-Cr-Zr alloys, which were obtained from the elemental analysis along the cylindrical box of 2 nm in diameter. In unirradiated alloy, the maximum concentration of Cr in the precipitate is about 30 at.%. The precipitate also includes Zr, Fe and Si. The concentration profiles of Zr and Si shows small peaks around the interface region between the precipitate and the matrix rather than inside the precipitate, suggesting the segregation of Zr and Si around the interfaces of Cr precipitate. After irradiation, the concentration profiles are very similar to those of unirradiated, thus almost no change are observed in the chemical composition and structure of the Cr precipitate after irradiation.

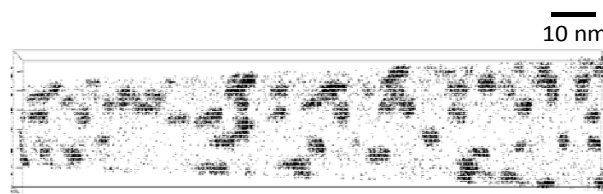


Fig.1. 3D atom map of Cr in the electron-irradiated Cu-Cr-Zr alloy.

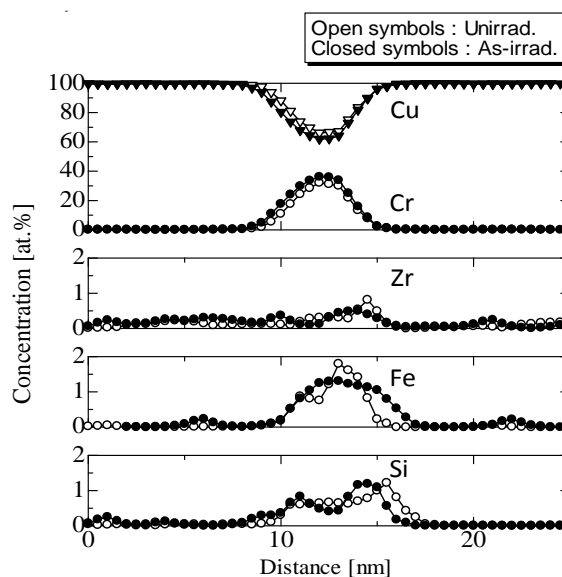


Fig.2. 1D concentration profiles of Cu,Cr,Zr,Fe and Si Around a Cr precipitate in the electron-irradiated and Unirradiated Cu-Cr-Zr alloy.

[1] Y. Nagai *et al.*, KUR Prog. Rep. (2010).

[2] M. Hatakeyama *et al.*, J. Nucl. Mater. , **386** (2009) 852.

[3] M. Hatakeyama *et al.*, Mater. Trans., **49**(3) (2008) 518.

## PR12-7 Defects Study for Bulk Metallic Glass Alloys Damaged by Electron Irradiation

F. Hori, N. Onodera, M. Maruhashi, A. Ishii, S. Mineno,  
A. Iwase, Q. Xu<sup>1</sup>, K. Sato<sup>1</sup> and T. Yoshiie<sup>1</sup>

Dept. of Mater. Sci., Osaka Prefecture University

<sup>1</sup>Research Reactor Institute, Kyoto University

**INTRODUCTION:** The bulk metallic glasses (BMGs) are expected to be useful for various applications due to their superior mechanical properties, hardness, strength, corrosion resistance and micro-formability [1-3]. The free volume in bulk metallic glass alloys has a significant effect on atomic relaxation and crystallization processes, although a detailed atomic configurations and their motion around free volume site has not been clarified yet. On the other hand, it can be deduced that high energetic particle irradiation affects the structure and various properties of bulk metallic glass. Positron annihilation is a unique technique and sensitive to detect the atomic size open volume in materials. In this study, we examined free volume change for  $Zr_xCu_{90-x}Al_{10}$  ( $x=50$  and  $60$ ) metallic glasses after energetic particles irradiations by positron annihilation lifetime and coincidence Doppler broadening techniques, in order to clear the radiation effects for various compositions of BMGs.

**EXPERIMENTS:** Two kinds of  $Zr_{50}Cu_{40}Al_{10}$  and  $Zr_{60}Cu_{30}Al_{10}$  bulk metallic glass with 8 mm in diameter and 60 mm in length was prepared by a tilt casting technique. For positron annihilation measurements, alloy sample was cut into the size of about 0.5 mm thickness. 8 MeV electron irradiations with total doses from  $4.0 \times 10^{17}$  to  $1.9 \times 10^{18}$  e/cm<sup>2</sup> was performed for these alloys at 300 K by LINAC at Research Reactor Institute, Kyoto University. Irradiated samples were examined by X-ray diffraction, positron annihilation lifetime and coincidence Doppler broadening measurements at room temperature.

**RESULTS:** Figure 1 shows X-ray diffraction results for before and after electron irradiation showing that crystallization dose not occurs. In this figure, it can be confirmed slight change of full width at half maximum by the irradiation. This is considered to be due to local atomic re-orientation. However, no crystallization occurs even at  $1.9 \times 10^{18}$  e/cm<sup>2</sup> irradiation. Fig. 2 shows the change in positron lifetime for each alloy after electron

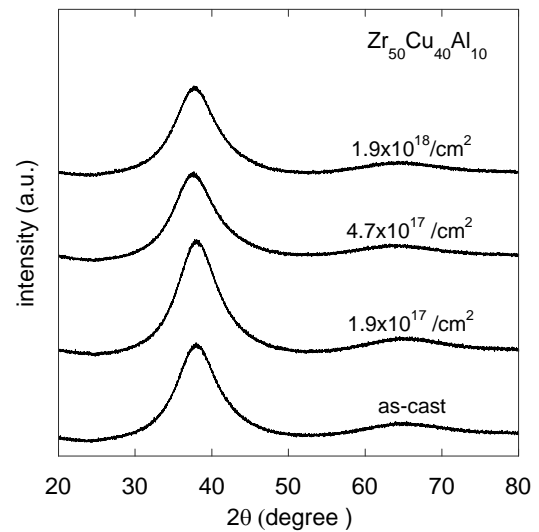


Fig. 1. XRD profiles for before and after 8MeV electron irradiated  $Zr_{50}Cu_{40}Al_{10}$  bulk metallic glass.

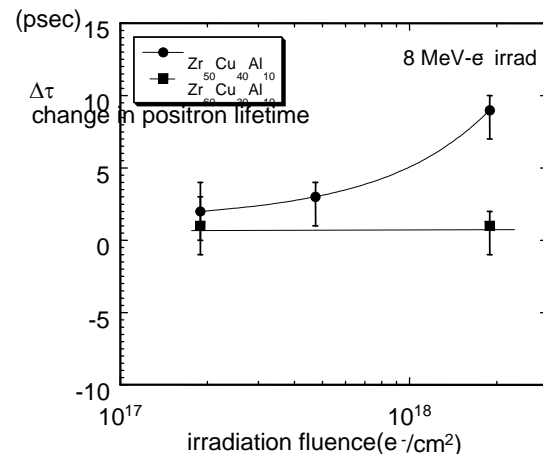


Fig. 2. Change in positron lifetime for each ZrCuAl bulk metallic glass as a function of electron irradiated fluence.

irradiation. Positron lifetime increases with increasing of irradiation dose in case for  $Zr_{50}Cu_{40}Al_{10}$ , but it remains constant for  $Zr_{60}Cu_{30}Al_{10}$  alloy. This composition dependence of free volume change by electron irradiation may be related to glass forming ability influencing thermal stability of local structure.

## REFERENCES

- [1] Inoue A 2000 Acta. Mater. **48** 279.
- [2] Löffler J F 2003 Intermetallics **11** 529
- [3] Johnson W L 2002 JOM. **54** 40

## PR12-8 Microstructure of Neutron Irradiated Vanadium Alloys in a Liquid Sodium Environment

K. Fukumoto, M. Iwasaki<sup>1</sup> and Q. Xu<sup>2</sup>

RINE, Univ. of Fukui

<sup>1</sup> Graduate school of Eng., Univ. of Fukui

<sup>2</sup> Research Reactor Institute, Kyoto University

**INTRODUCTION:** In order to understand the thermal stability of defect clusters, and investigate a recovery method for irradiation hardening and embrittlement, post-irradiation annealing experiments are performed to evaluate the recovery of microstructure and mechanical properties of vanadium alloys irradiated below 300°C.

In this study, experiments to determine the influence of post-irradiation annealing on mechanical properties and microstructures in neutron-irradiated V-Cr-Ti alloys are described. Two groups of specimens (as-irradiated specimens and specimens which underwent the post-irradiation annealing treatment) were subjected to tensile tests at room temperature and 500°C. Post-irradiation annealing experiments with long intervals of up to 50 hr were used to recover the original strength and ductility.

**EXPERIMENTS:** The majority of test specimens for this study were prepared from V-4Cr-4Ti alloys. The tensile specimens had nominal gauge dimensions of 0.25mm(t) x 1.2mm(w) x 5mm(l). Before irradiation, all specimens were annealed in vacuum at 1000°C for 2hrs. The specimens were irradiated at 228°C to 280°C with 3 to 5 displacements per atom (dpa) in the ATR-A1 or at 306°C with 6 dpa in the HFIR-11J. Post-irradiation annealing was carried out for 2 to 50 hr at 500°C and 600°C in a vacuum. Tensile tests were conducted at room temperature and 500°C. TEM samples were punched from non-deformed areas of tested specimens. The microstructural TEM observations were performed in KUR/Kyoto Univ.

**RESULTS:** As-irradiated V-4Cr-4Ti alloys in ATR-A1 and HFIR-11J showed the reduction of ductility below 1% and remarkable irradiation hardening above 700MPa in RT tensile tests. Figure 1 shows the stress-strain curves of annealed V-4Cr-4Ti alloys after neutron irradiation at 300°C with damage level of 6dpa in HFIR. From left to right, annealing time of irradiated V-4Cr-4Ti alloys increases from 0, 10h, 20h and 50h. A recovery of ductil-

ity to 3% and hardening to 500MPa could be observed in an annealed V-4Cr-4Ti alloy at 600°C for 2hrs. On the other hand, no typical changes in uniform elongation and yield stress increase could be seen in an annealed one at 500°C for 2hrs in tensile test. The V-4Cr-4Ti alloys annealed at 500°C for 20hrs showed no change of yield stress increase compared to as-irradiated one in the tensile test at RT, but the total elongation was recovered to 5% with the stress-strain curve like complete elasto-plastic behavior. Even at 500°C tensile test, recovery of ductility could be seen in annealed sample at 500°C for 20hrs. In the case of annealed sample for 50hrs, the ultimate tensile strength decreased significantly with 5% of uniform elongation. From the microstructural observation of annealed samples, a dense of tiny defect clusters and tangled dislocation were observed in the as-irradiated sample. However as annealing time increased, reduction of defect cluster density and growth of defect clusters as dislocation loops could be seen. The recovery of defect clusters did not correspond to the recovery of yield stress and ultimate tensile strength because the tensile stress does not seem to be affected by the microstructural changes from the calculation of Orowan stress increase of each microstructure such as dislocation, loop and precipitates. It was found that the recovery of mechanical behavior can be appeared after 10 hour anneal at 500°C in order to improve the low-temperature irradiation embrittlement behavior of V-4Cr-4Ti alloys

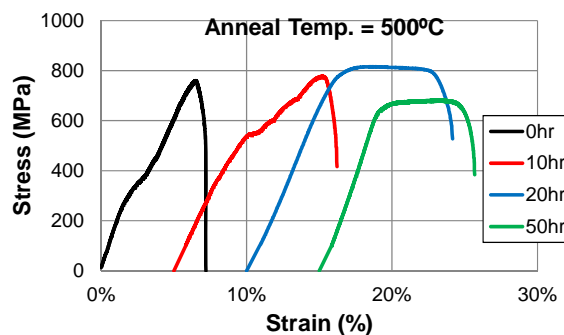


Fig. 1. Stress-Strain curves of annealed V-4Cr-4Ti alloys after neutron irradiation at 300°C with damage level of 6dpa in HFIR. From left to right, annealing time of irradiated V-4Cr-4Ti alloys increases from 0hr, 10hr, 20hr and 50hr.

I. Mukouda\*, K. Yamakawa<sup>1</sup>, T. Yoshiie<sup>2</sup> and Q. Xu<sup>2</sup>

Hiroshima International University

<sup>1</sup>Faculty of Engineering, Ehime University

<sup>2</sup>Research Reactor Institute, Kyoto University

**INTRODUCTION:** A structural ordering of atoms in Au<sub>3</sub>Cu alloys has been investigated by the electrical resistivity measurements. The measuring temperature dependence of isothermal resistance curve has been investigated experimentally during ordering. The rate of ordering is slow because of low critical temperature of Au<sub>3</sub>Cu alloy. Therefore, in many investigations, the rate was considerably enhanced by the quenching of the specimen from high temperatures. In the present experiment the electrical resistances of the Au<sub>3</sub>Cu alloy are measured at various temperatures during ordering and quenching temperature dependence of the isothermal annealing curve is studied.

**EXPERIMENTS:** The specimen was set in a stainless steel tube, which was enclosed argon or helium gas after the setting, for annealing. The electrical resistance was measured during the annealing at 150°C and measured at iced water. After each annealing, the tube was quickly pulled out from the furnace and put into the iced water. Therefore, the resistance is measured at the same structural condition as it at 150°C. The resistance measurement was done by standard four probe method.

**RESULTS:** The electrical resistance changes during isothermal annealing at 150°C after quenching are shown in Fig.1 for various quenching temperatures ( $T_Q$ ). The isothermal resistance curves, which are measured at 150°C and 0°C are shown. Full and open marks show the data at 150°C and 0°C, respectively. For low quenching temperatures, the curves increase and then decrease with the resistance maximums during annealing. For high quenching temperatures, the curves decrease with the annealing time. Dissipation of the resistance maximums on the curves for the high quenching temperature is caused by the shift of the curves to direction of shorter annealing time.

Even after the quenching, similar behavior of the time position of maximum is observed on the isothermal annealing curves: i.e. The annealing time at the resistance maximum decreases with the measuring temperature ( $T_M$ ) decrease for the low quenching temperatures.

The rate of resistance change for each measuring temperature increases with the quenching temperature. If the atoms diffuse by vacancy mechanism, the jump rate of atom,  $J$  is calculated using the formula

$$J = Avc \exp(-E_m/kT), \quad (1)$$

where  $A$ ,  $v$ ,  $c$ ,  $E_m$ ,  $k$  and  $T$  are a constant, an effective frequency for the vibration of the atom in the direction of the saddle point, a vacancy concentration, the vacancy migration energy, Boltzmann's constant and the absolute temperature[1]. If vacancy concentration is obtained, the isothermal resistance curves can be calculated using the above equation (1). Using the vacancy concentration of pure Au the resistance curves are calculated and shown in Fig.1 with dotted curve and dot dashed curve for  $T_Q=700^\circ\text{C}$  and  $850^\circ\text{C}$ , respectively, because reliable vacancy concentration in quenched Au<sub>3</sub>Cu alloy is not known. The curves for  $T_Q=550^\circ\text{C}$  are taken as a base on the calculation. The calculated curves largely deviate from experimental curves especially in the range of long annealing time even using the maximum vacancy concentrations at  $T_Q$ . In partly the disagreement may be improved by the ordering during the quenching. In fact, the electron diffraction pattern at as quenched state shows stronger order spots for higher quenching temperature as shown in Fig.2.

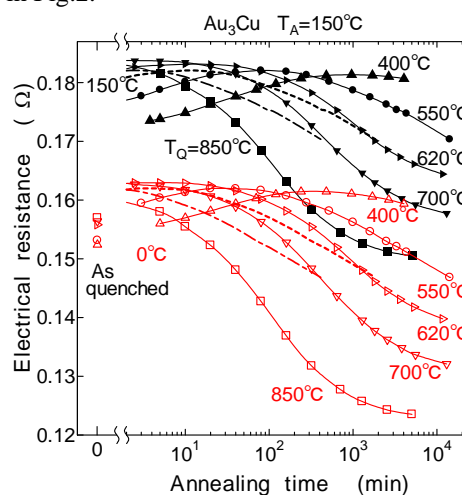


Fig. 1. Iso-thermal annealing curves of Au<sub>3</sub>Cu.

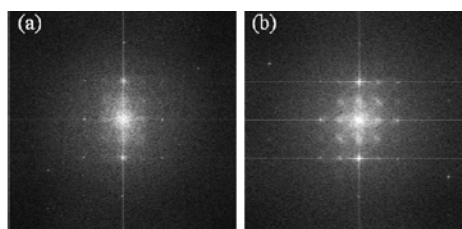


Fig.2. Calculated FFT Pattern of As quenched Au<sub>3</sub>Cu  
(a)  $T_Q=400^\circ\text{C}$  (b)  $T_Q=700^\circ\text{C}$ .

### REFERENCES:

- [1] A.C. Damask, G.J. Dienes: Point Defects in Metals, Goldon and Breach Science, New York, 1963, chap.3

## PR12-10 Effects of Thermal Aging on Mechanical Properties of Fe-Cr Ferritic Alloys

R. Kasada<sup>1</sup>, Y. Sakamoto<sup>2</sup>, K. Yabuuchi<sup>2</sup>, A. Kimura<sup>1</sup>,  
K. Sato<sup>3</sup>, Q. Xu<sup>3</sup> and T. Yoshiie<sup>3</sup>

<sup>1</sup>Institute of Advanced Energy, Kyoto University

<sup>2</sup>Graduate School of Energy Science, Kyoto University

<sup>3</sup>Research Reactor Institute, Kyoto University

**INTRODUCTION:** Oxide dispersion strengthened (ODS) ferritic steels are expected to be used for the first-wall component in the fusion reactors as well as the fuel pin cladding in the Generation IV nuclear fission systems [1]. However, such high-Cr steels may suffer from thermal aging embrittlement, which is well-known 475 °C embrittlement, due to phase separation of Fe and Cr. In the previous study [2], we applied a positron annihilation spectrometry to detect the phase separation in the high-Cr ODS steels as well as in the non-ODS ferritic steel. As shown in Fig.1, the positron trapping behavior in the thermally-aged Fe-16Cr ODS ferritic steel is slightly affected by the thermal aging at 400°C up to 2400 h. But the trapping site is still unclear for the thermally-aged and un-aged ODS ferritic steels. After these results, currently, Kasada and Sato are widely investigating the positron trapping behavior in the Fe-Cr alloys under “the Strategic Promotion Program for Basic Nuclear Research by the Ministry of Education, Culture, Sports, Science and Technology of Japan”. So the present collaborative research has moved to investigate the neutron irradiation effect on the phase separation of Fe-Cr ferritic alloys. In the FY2010 we have obtained the nano-indentation hardness data of Fe-Cr binary alloys before and after thermal aging at 475 °C as a reference data for the neutron irradiation in KUR scheduled in FY2011.

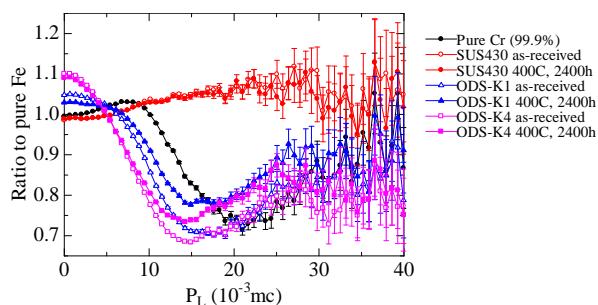


Fig. 1. Positron CDB ratio-curves obtained for the ODS steels and SUS430 before and after thermal aging at 400 °C up to 2400 h.

**Experimental Procedure:** Materials used in the present study is Fe-Cr binary alloys. Thermal aging treatment on these materials was carried out at 475 °C up to 100 h. Nano-indentation hardness tests were performed using Nano-Indenter G200 with a continuous stiffness measurement method to obtain the hardness depth profile.

**Results and Discussions:** The depth profile of nano-indentation hardness in the Fe-Cr alloys before and after the thermal aging was measured up to a depth of approximately 1.5 μm. Based on the application of Nix-Gao model [3], the results were converted to a bulk-equivalent hardness,  $H_0$ , which can be related to the Vickers hardness. As shown in the Fig. 2, the Cr-dependence of the  $H_0$  is very similar to that of the micro-Vickers hardness obtained for the similar materials [4]. These data sets will be provided for the reference data of the neutron irradiation experiments.

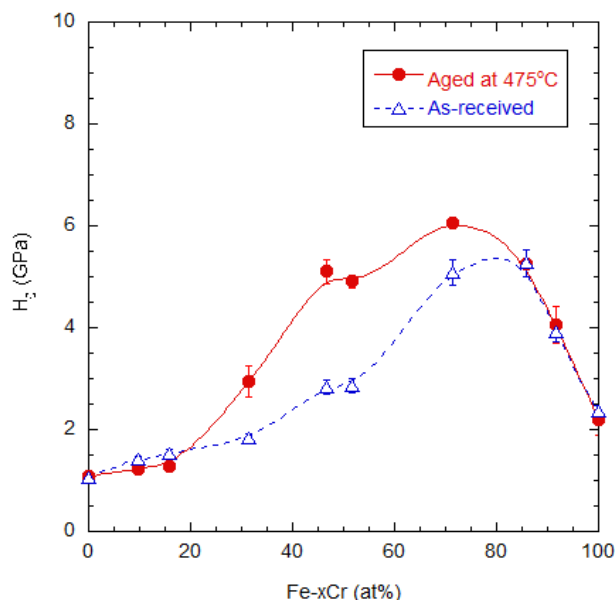


Fig. 2. Cr-dependence of a bulk-equivalent hardness,  $H_0$ , converted from nano-indentation hardness of Fe-Cr binary alloys before and after the thermal aging at 475 °C up to 100 h.

### REFERENCES

- [1] A. Kimura, *et al.*, Journal of Nuclear Science and Technology, 44 (2007) 323-328.
- [2] R. Kasada *et al.*, KURRI progress report 2009.
- [3] R. Kasada *et al.*, Fusion Engineering and Design, in press.
- [4] R. Kasada and K. Sato, to be submitted.

H. Tsuchida, A. Itoh<sup>1</sup>, K. Satoh<sup>2</sup>, T. Yoshiie<sup>2</sup> and Q. Xu<sup>2</sup>

Quantum Science and Engineering Center, Kyoto University

<sup>1</sup>Department of Nuclear Engineering, Kyoto University

<sup>2</sup>Research Reactor Institute, Kyoto University

**INTRODUCTION:** Materials of fusion reactors or nuclear reactors continuously undergo radiation damaging effects. Production of radiation defects and their accumulation are induced, resulting in a change of microstructure in materials. A nanocrystalline material with grain size of less than a few tens micrometers is known to have high resistance to radiation damaging effects because its grain boundary acts as effective sinks that absorb radiation-induced defects. A recent simulation has showed a new mechanism of radiation resistance in nanocrystalline materials: self-healing of radiation damage occurs via interstitial emission near grain boundary [1].

In this work, we studied microstructure of nanocrystalline Ni by thermal desorption spectra (TDS) analysis and positron annihilation spectroscopy.

**EXPERIMENTS:** Samples were nanocrystalline Ni purchased from Goodfellow Corp.. An average grain size of the samples measured by 200kV transmission electron microscope was about 30 nm. To investigate microstructure of the sample, hydrogen was loaded into the sample by charging with high-pressured hydrogen gas. We performed measurements of positron annihilation lifetime spectroscopy (PALS) and also TDS analysis for sample before and after loading hydrogen.

**RESULTS:** Results of the PALS were listed in Table 1. Values of the short lifetime and its intensity were about 146 ps and about 80 %, respectively, for samples before and after loading hydrogen. The lifetime component corresponds to that positrons annihilate at inside of the grain. On the other hand, a value of the long lifetime for the hydrogen-loaded sample was longer than that for non-loaded sample. The result suggests that hydrogen is loaded into the grain boundary. In order to confirm this suggestion, TDS analysis was carried out for nanocrystalline and annealed coarse-grained (or defect free) Ni samples, which were charged with hydrogen. The result is shown in Fig. 1. For the nanocrystalline sample the number of loaded hydrogen atoms was  $7.77 \times 10^{16}$  per 1g sample. This value is larger than that for the annealed sample. This indicates that most of the hydrogen atoms are likely to trap into grain boundary of nanocrystal. One can see some peaks in the TDS spectra. The peak around about 400K and 500K are due to hydrogen emission from grain boundary and from inside of grains, respectively. In order to understand trapping site of hydrogen atoms in

nanocrystalline materials in more detail, it is necessary to perform further experiments on the microstructure studies of the nanocrystalline materials irradiated with neutrons and high-energy ions by combined analysis of TDS and PALS.

Hydrogen load	Mean lifetime [ps]	Two component analysis	
		Lifetime [ps]	Intensity [%]
Before	180	149±1 (short) 309±6 (long)	81±1 19±1
After	169	144±2 (short) 292±12 (long)	84±2 16±2

Table 1. Experimental results of positron lifetime and its intensity for samples before and after loading hydrogen.

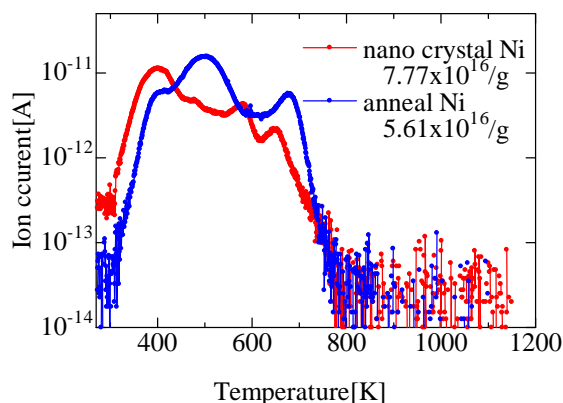


Fig. 1. Experimental results of TDS spectra for hydrogen-loaded samples of nanocrystalline and annealed Ni.

#### REFERENCES:

- [1] Bai *et al.*, "Effective annealing of radiation damage near grain boundaries via interstitial emission", *Science* **327** (2010) 1631

K. Sato, K. Takeyasu, Q. Xu, K. Mori and T. Yoshiie

*Research Reactor Institute, Kyoto University*

**INTRODUCTION:** Nuclear energy is important in energy system and is expected to remain so in the future. Accelerator driven system and fusion reactor are important option for nuclear energy. Nuclear materials are used under high-energy particle irradiation, and they are heavily irradiated in spallation neutron source and fusion reactor. The irradiation-resistant materials are needed for them.

Voids are major defects in irradiated materials and induce embrittlement [1,2]. Gas atoms produced by nuclear transmutation promote the nucleation and growth of voids. Helium and hydrogen are formed by (n,  $\alpha$ ) and (n, p) reactions, respectively. Therefore, interaction between defects and gas atoms is very important.

In this study, strength of binding between vacancy type defects and deuterium are investigated by positron annihilation spectroscopy.

**EXPERIMENTS:** The purity of the nickel plate used was 99.9999% (Johnson-Matthey). The specimens were prepared from cold-rolled sheets (0.2 mm in thickness) by punching (5 mm in diameter) followed by annealing at 1173 K for 1 h in a vacuum.

Electron irradiation was performed by an electron linear accelerator of Research Reactor Institute, Kyoto University with an acceleration voltage of 8 MV at room temperature. This irradiation introduces Frenkel pairs, and interstitials diffuse and disappear faster than vacancies. As a result, residual defects are mainly vacancy type defects. Quenching from 1573K to 273K was also performed. After introducing defects, high pressure deuterium charge was performed under 3 MPa and 373 K.

Positron annihilation lifetimes of specimens were measured by using conventional fast-fast spectrometer with a time resolution of 190 ps (full width at half maximum) and each spectrum was accumulated to a total of  $1 \times 10^6$  counts.

**RESULTS:** Figure 1 shows the isochronal annealing behavior of positron annihilation lifetime of electron-irradiated and deuterium-charged Ni. Figure 2 shows the isothermal annealing behavior of positron annihilation lifetime of quenched and deuterium-charged Ni. The positron lifetime  $\tau_2$  of about 170 ps and 210 ps denotes the existence of single vacancies and 3 vacancy clusters, respectively.  $\tau_2$  decreased after deuterium charging. Vacancy type defects absorb deuterium atoms and this leads to the decrease of  $\tau_2$ . After 243 K annealing,  $\tau_2$  started to increase in Fig. 1. From this tendency, the binding energy of single vacancy and deuterium was 0.40 eV.  $\tau_2$  started to change after 14 h annealing in Fig. 2. From this tendency, the binding energy of 3 vacancy clusters and deu-

terium was 0.65 eV. These values are almost the same as previous works (0.44 eV [4] and 0.73 eV [5]).

Deuterium trapped at vacancy type defects was detected by positron annihilation lifetime measurements.

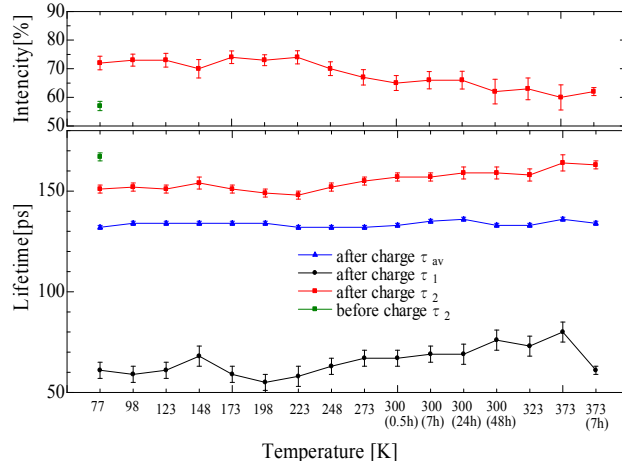


Fig. 1. Isochronal annealing behavior of positron annihilation lifetime of electron-irradiated and deuterium-charged Ni. Measurements were performed at liquid nitrogen temperature.

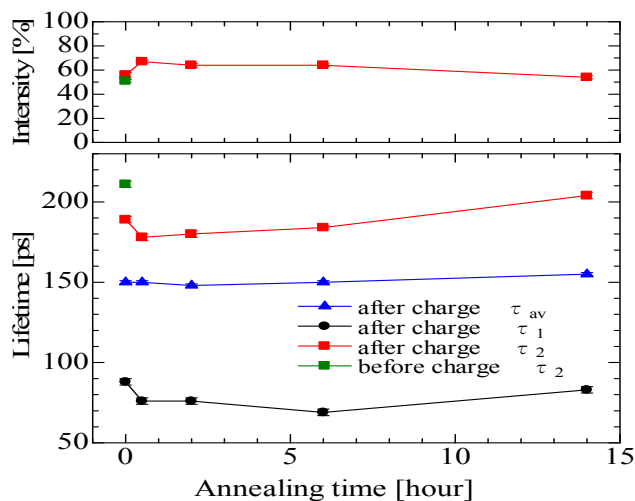


Fig. 2. Isothermal (room temperature) annealing behavior of positron annihilation lifetime of quenched and deuterium-charged Ni. Measurements were performed at about 200 K.

### REFERENCES:

- [1] F.A. Garner, Materials Science and Technology, Vol. 10 (VCH Weinheim, 1994), p. 419.
- [2] T. Okita *et al.*, J. Nucl. Mater. 307–311 (2002) 322.
- [3] B.L. Shivachev *et al.*, J. Nucl. Mater. 306 (2002) 105.
- [4] C. Szeles *et al.*, J. Phys. F 17 (1987) 2031.
- [5] A.P. Druzhkov *et al.*, Phys. Stat. Sol. A205 (2008) 1546.

K. Tokunaga, K. Araki, T. Fujiwara, Y. Miyamoto,  
Q. Xu<sup>1</sup> and T. Yoshiie<sup>1</sup>

*Research Institute for Applied Mechanics,  
Kyushu University*

<sup>1</sup>*Research Reactor Institute, Kyoto University*

**INTRODUCTION:** Tungsten materials are potential candidates of the divertor armor and first wall materials of the next fusion devices due to their very low erosion yield and high temperature properties. However, heat load, hydrogen and helium atoms from the plasma, which affect on damage accumulation and mechanical properties, may reduce these superior properties of tungsten. Hydrogen or helium single beam irradiation experiments have been performed to investigate the synergistic effects of the heat loading and the particle loads (hydrogen or helium) on modification of tungsten. Surface modification by helium and hydrogen beam heating is completely different from results of electron beam heating. In particular, helium beam heating causes remarkable surface modification such as the fine-scale, rough surface at high temperatures due to strong interaction with helium and lattice defects. This modification may influence thermal properties such as thermal conductivity, mechanical properties and tritium retention of the material. Simultaneous irradiation of hydrogen and helium beam has been investigated. However, the armor materials are simultaneously exposed to high heat flux hydrogen isotopes and helium as well as electrons. Very little information is available on the combined effects of high heat flux hydrogen and helium particle implantation under the high heat loading. In the present study, high heat flux hydrogen and helium mixture beam irradiation experiments have been performed to investigate the synergistic effects simultaneous implantation of high heat flux hydrogen and helium on modification and hydrogen retention of tungsten materials.

**EXPERIMENTS:** Samples used in the present experiments are powder metallurgy tungsten (PM-W) and ultra fine grain W-0.5wt%TiC alloy with MA in H<sub>2</sub> which is noted by W-0.5 wt%TiC-H<sub>2</sub>. The W-TiC alloy have been developed for good resistance of radiation damage due to neutron irradiation and high temperature

embrittlement. Sizes of the PM-W, with size 20x20x5 mm and 10x10x1mm were used. Purity of PM-W was 99.99%. Size of W-TiC alloy was 10x10x1 mm. The sample surfaces were electropolished. The samples are mechanically mounted on a Cu holder, actively water cooled and are repeatedly irradiated by hydrogen and helium mixture beam (18 keV,  $\sim 2 \times 10^{21}/\text{m}^2\text{s}$ ,  $\sim 7\text{MW}/\text{m}^2$ , 1.5~3s) up to a fluence of the orders between  $10^{22}$  and  $10^{24}/\text{m}^2$  using the Divertor Acceptance Testing System (DATS) in JAEA.

**RESULTS:** The surface temperatures gradually increase and reach a peak temperatures and starts to decrease after beam turn-off. Temperature changes also depend on the size of the samples, heat flux and thermal contact with the sample and the Cu holder. In the case of PM-W, surface modification such as micro-relief occurs and corresponds to the grains from 10 to 100 nm. As the sputtering depends on the grain orientation, the surface modification may be formed by micro-structure change near the surface and erosion due to the sputtering. In addition, grain dependence on modification by hydrogen-helium irradiation is relatively small. It is clearly seen that surface modification due to the mixture beam irradiation is different from that of the single hydrogen and helium beam irradiation in the case of W-0.5 wt%TiC-H<sub>2</sub> alloy. Small holes with a diameter of a few 100 nm are observed. These holes may be formed by ex-foliation of grains due to embrittlement by helium irradiation. On the other hand, in the case of mixture beam irradiation, surface is relatively smooth comparing with the single beam irradiation.

**CONCLUSION:** High heat flux hydrogen and helium mixture beam irradiation experiments have been performed to investigate the synergistic effects simultaneous implantation of high heat flux hydrogen and helium on modification and hydrogen retention of tungsten materials. Surface modification by hydrogen-helium mixture beams is completely different from results of single beam irradiation. In particular, mixture beam irradiation causes remarkably high hydrogen retention. Therefore, surface modification, erosion and hydrogen isotope retention will be evaluated in consideration of helium simultaneous irradiation.